Chemosphere 324 (2023) 138322

Contents lists available at ScienceDirect

Chemosphere

journal homepage: www.elsevier.com/locate/chemosphere

Photo-electrocatalytic based removal of acetaminophen: Application of visible light driven heterojunction based $BiVO_4$/BiOI photoanode

Agha Zeeshan Ali [a,*], Yiqian Wu [a], Yasmina-Doekhi Bennani [b], Henri Spanjers [a], Jan Peter van der Hoek [a,c]

[a] Department of Water Management, Faculty of Civil Engineering and Geosciences, Delft University of Technology, P.O Box 5048, 2600, GA, Delft, the Netherlands
[b] Nijhuis Water Technology B.V, Innovatieweg 4, 7007 CD, Doetinchem, the Netherlands
[c] Waternet, Department of Research & Innovation, P.O. Box 94370, 1090, GJ, Amsterdam, the Netherlands

HIGHLIGHTS

- Electrode deposition process for the successful fabrication of photoanodes.
- Increase in absorbance area and quantum efficiency by combing $BiVO_4$ and BiOI.
- In-situ generation of hydroxyl and super-oxide radicals by $BiVO_4$/BiOI photoanode.
- 87% removal of acetaminophen (40 μg L^{-1}) by $BiVO_4$/BiOI photoanode.

GRAPHICAL ABSTRACT

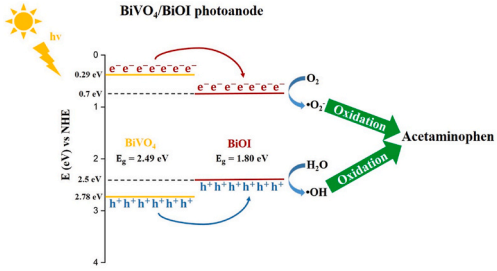

ARTICLE INFO

Handling Editor: E. Brillas

Keywords:
Organic micro-pollutants
Advanced oxidation process
Photoelectrocatalysis
Heterojunction photoanodes
$BiVO_4$/BiOI
Acetaminophen

ABSTRACT

The presence of organic micro-pollutants (OMPs) in wastewater treatment effluents is becoming a major threat to the water safety for aquatic and human health. Photo-electrocatalytic based advanced oxidation process (AOP) is one of the emerging and effective techniques to degrade OMPs through oxidative mechanism. This study investigated the application of heterojunction based $BiVO_4$/BiOI photoanode for acetaminophen (40 μg L^{-1}) removal in demineralized water. Photoanodes were fabricated by electrodeposition of $BiVO_4$ and BiOI photocatalytic layers. Optical (UV–vis diffusive reflectance spectroscopy), structural (XRD, SEM, EDX) and opto-electronic (IPCE) characterization confirmed the successful formation of heterojunction for enhanced charge separation efficiency. The heterojunction photoanode showed incident photon to current conversion efficiency of 16% (λ_{max} = 390 nm) at an external voltage of 1 V under AM 1.5 standard illumination. The application of the $BiVO_4$/BiOI photoanode in the removal of acetaminophen at 1 V (external bias) vs Ag/AgCl under simulated sunlight showed 87% removal efficiency within the first 120 min compared to 66% removal efficiency of the $BiVO_4$ photoanode. Similarly, combining $BiVO_4$ and BiOI exhibited 57% increase in first order removal rate coefficient compared to $BiVO_4$. The photoanodes also showed moderate stability and reusability by showing 26% decrease in overall degradation efficiency after three cycles of each 5 h experiment. The results obtained in this study can be considered as a stepping stone towards the effective removal of acetaminophen as an OMP present in wastewater.

* Corresponding author. Department of Water Management, Faculty of Civil Engineering and Geosciences, Delft University of Technology, P.O Box 5048, 2600, GA, Delft, the Netherlands.
E-mail address: a.aghzeeshan@tudelft.nl (A.Z. Ali).

https://doi.org/10.1016/j.chemosphere.2023.138322
Received 10 November 2022; Received in revised form 3 March 2023; Accepted 4 March 2023
Available online 6 March 2023

1. Introduction

Water pollution is a major environmental concern due to various factors among which increase in industrial growth, population growth and water scarcity are the most important (Rogowska et al., 2020). Owing to the importance of water safety, The United Nations (UN) also included access to clean water and sanitation in its sustainable development goals list ("THE 17 GOALS | Sustainable Development," n.d.). Keeping the surface water bodies safe for use is imperative because major part of the drinking water supply comes from surface water resources (van der Hoek et al., 2014). The majority of the research efforts within wastewater treatment domain is focused on ensuring that the wastewater treatment plant's (WWTP) effluent is safe for aquatic and human life (Corominas et al., 2013). Apart from resource recovery from the wastewater (Puyol et al., 2017; Solon et al., 2019), using the treated wastewater for different practical purposes is also becoming increasingly important within the circular economy domain (Smol et al., 2020). Conventional treatment plants only remove carbon (C), nitrogen (N) and phosphorous (P) from the wastewater (Neczaj and Grosser, 2018). However, over the past several decades analysis of WWTP effluents has shown that some chemical compounds mainly belonging to the industrial and pharmaceutical compounds category (Petrie et al., 2015) are still present in the effluent within the range of 1–10 μg L^{-1} (Ratola et al., 2012). The compounds that are present in the water resources in the ng L^{-1} to μg L^{-1} range are called micro-pollutants (MPs), and MPs that are organic are called organic micro-pollutants (OMPs) (Golovko et al., 2020).

Advanced oxidation processes (AOPs) are becoming increasingly important for the complete removal of OMPs from industrial or municipal wastewater. Among various types of AOPs, photo-electrocatalytic (PEC) based AOP is gaining importance due to the use of solar energy to activate photocatalytic materials for the generation of reactive species. PEC based AOP involves the use of semiconducting anode materials for the in-situ production of oxidants that are mainly hydroxyl (•OH) and superoxide radicals ($^{\bullet}O_2^-$). The in-situ oxidants unselectively oxidize the organic pollutants to remove them from the wastewater (Garcia-Segura and Brillas, 2017). Metal oxide based photocatalysts such as titanium dioxide (TiO_2) (Collivignarelli et al., 2021), tungsten trioxide (WO_3) (Liao et al., 2021), zinc oxide (ZnO) (Rajeswari and Venckatesh, 2021), zirconium dioxide (ZrO_2) (Sponza and Oztekin, 2016) and iron oxide (Fe_2O_3) (Aragaw et al., 2021) are widely reported in literature for the removal of pharmaceuticals and industrial dyes (1–10 mg L^{-1}) in aqueous solution. However, these photocatalysts have an intrinsic drawback that due to their large band gap energy (3.0–3.5 eV) they can only absorb photons in the UV range of solar irradiation. Bismuth vanadate ($BiVO_4$) in its monoclinic scheelite phase is a small band gap (~2.4 eV) visible light driven photocatalyst and, due to its stability and non-toxicity, $BiVO_4$ is used as anodic material for the PEC based removal of organic micro-pollutants in aqueous solution (Deshpande et al., 2020; Shao et al., 2020a). However, PEC activity of pristine $BiVO_4$ is hindered due to poor charge transport and high rate of recombination of photo-generated electron-hole pairs (Orimolade and Arotiba, 2020a). The PEC activity corresponds to the removal efficiency of the $BiVO_4$ photoanode for the removal of pollutants from aqueous solution. Combining monoclinic scheelite $BiVO_4$ with other photocatalysts to make a heterojunction is one of the effective strategies to improve the PEC activity of $BiVO_4$ (Orimolade and Arotiba, 2020a). Depending on the band gap alignment of the photocatalysts under consideration, the heterojunction between them can be of two types, either type I or type II (Orimolade and Arotiba, 2020b). Photogenerated holes and electrons in type I heterojunction are transferred to the electrode-electrolyte interface, whereas in type II heterojunction the photogenerated charge carriers are transferred in opposite directions thereby effectively enhancing the charge separation in the photoanode (Orimolade and Arotiba, 2020b) (illustrated in Fig. 1). Various heterojunction structures that are mostly type II such as $WO_3/BiVO_4$ (Du et al., 2019, p. 3), $CuO/BiVO_4$ (Bai et al., 2018), $CdS/BiVO_4$ (Li et al., 2018), $BiVO_4/Ag_2S$ (Orimolade and Arotiba, 2020c) and $BiVO_4/Ag_3PO_4$ (Cao et al., 2018) are reported in literature that have shown enhanced PEC based removal of dyes and pharmaceutical compounds compared to pure $BiVO_4$.

Bismuth oxyiodide (BiOI) is also a bismuth based small band gap (~1.9 eV) photocatalyst that can be used for visible-light applications. Combining $BiVO_4$ with BiOI is also possible as $BiVO_4$/BiOI heterojunction based nanoparticles are used to remove dyes. The heterostructure based $BiVO_4$/BiOI nanoparticles shows improved PEC activity compared to pristine $BiVO_4$ and BiOI due to enhanced charge separation efficiency (He et al., 2016; Ni et al., 2018). Only one application of $BiVO_4$/BiOI photoanode is reported in literature for the degradation of pharmaceuticals (Orimolade et al., 2019a), however, the concentration of pharmaceuticals was 10 mg L^{-1}, which is much higher than actual concentration of OMPs present in the aquatic environment (Golovko et al., 2020). At lower concentrations (<100 μg L^{-1}) the removal kinetics of organic micro-pollutants would be different as there will be chances of lack of diffusion of organic molecules from bulk solution to the surface of the photoanode. To the best of our knowledge and based on a literature review (Orimolade and Arotiba, 2020b), there is a lack of knowledge regarding the use of $BiVO_4$ and $BiVO_4$/BiOI photoanode for the removal of organic micro-pollutants in the concentration range of 0–100 μg L^{-1}.

Acetaminophen (ACT) belongs to the non-steroidal anti-inflammatory drugs (NSAIDs) category that can be purchased as over the counter (OTC) drug without any specific prescription (Sajid et al., 2022). Due to the excessive use of ACT for pain and fever reduction (Chowdhury et al., 2021), it is one of the most commonly found OMP in wastewater, surface water and drinking water (Phong Vo et al., 2019). Eco-toxic effects of ACT and its transformation products on aquatic and human life have been widely investigated and now ACT is recognized as an environmental and human health concern (López Zavala et al., 2020). Conventional WWTPs are unable to completely remove ACT from the influent and a concentration between 0 and 20 μg L^{-1} is still present in the WWTPs effluent in many European countries (Lee et al., 2020). Electrochemical AOP (eAOP) has been widely employed to remove ACT from secondary effluents of WWTPs and simulated wastewater within the range of 1–10 mg L^{-1} (Ouarda, 2020). However, there is a lack of information available on the removal kinetics of ACT at lower concentrations (<100 μg L^{-1}) using photo-electrocatalysis (PEC).

The objective of this study was to successfully fabricate a visible light driven heterojunction $BiVO_4$/BiOI photoanode and to employ it for ACT (40 μg L^{-1}) removal in demineralized water. Removal kinetics of ACT by using the $BiVO_4$/BiOI photoanode was also compared with pristine $BiVO_4$ and BiOI photoanodes. $BiVO_4$, BiOI and $BiVO_4$/BiOI photoanodes were fabricated by electrodeposition. Fabricated photoanodes were characterized by using structural, morphological, optical and opto-electronic characterization techniques to analyse and confirm the formation of heterojunction between $BiVO_4$ and BiOI. Lastly, the fabricated photoanodes were used to remove ACT in demineralized water in a three electrode PEC set-up. Quenching experiments were also performed by using methanol and p-benzoquinone (p-BZQ) to evaluate the role of reactive species ($^{\bullet}OH$ and $^{\bullet}O_2^-$) in $BiVO_4$/BiOI photoanode based ACT removal.

2. Materials and methods

Three different kinds of photoanodes (BiOI, $BiVO_4$ and $BiVO_4$/BiOI) were prepared in the first stage and their fabrication processes are described below.

2.1. Fabrication of BiOI photoanode

As previously reported, electrodeposition (Kim and Choi, 2014; Orimolade and Arotiba, 2020c) with minor adjustments was used to

deposit BiOI on fluorine doped tin oxide (FTO) glass (40 mm × 40 mm x 2.2 mm). To prepare the electrolyte for electrodeposition, 0.04 M bismuth nitrate pentahydrate ($Bi(NO_3)_3{\cdot}5H_2O$) was added to 50 mL of 0.4 M potassium iodide (KI) solution and the pH was adjusted to 1.5–1.6 by using 1 M HNO_3. This solution was mixed with 20 mL of ethanol (100%) containing 0.23 M p-benzoquinone and sonicated afterwards for 10–15 min. To electrodeposit the BiOI layer on the FTO glass, a cathodic bias of −0.2 V was applied for 5 min to the working electrode in a three electrode electrochemical cell. FTO glass, Ag/AgCl (3.0 M KCl) electrode and a platinum wire were used as the working electrode, reference electrode and counter electrode, respectively. After 5 min the working electrode was taken out from the cell and was rinsed with de-ionized water. After drying, a bright red coloured BiOI photoanode (shown in supplementary Fig. 2) was stored for further use.

2.2. Preparation of $BiVO_4$ photoanode

A $BiVO_4$ photoanode was prepared by converting the BiOI layer to $BiVO_4$. First the BiOI layer on the surface of FTO glass (40 mm × 40 mm x 2.2 mm) was electrodeposited in the same way as described in the above section (2.1). To convert the BiOI layer to $BiVO_4$ a 0.15–0.2 mL of Dimethyl Sulfoxide (DMSO) solution containing 0.2 M Vanadyl-Acetylacetonate was drop casted on the BiOI layer. Then, the electrode was placed in a furnace for annealing treatment at 450 °C for 2 h (ramping rate at 5 °C/min). After annealing treatment, the electrode was taken from the furnace and as a last step the electrode was soaked in 1.0 M NaOH for 15 min under gentle stirring to remove the excess vanadium oxide (V_2O_5). After removing excess V_2O_5, the bright yellow coloured electrode (shown in supplementary Fig. 2) was kept in a dry place under normal atmosphere for further use.

2.3. Fabrication of $BiVO_4$/BiOI heterojunction photoanode

To fabricate a heterojunction photoanode, first $BiVO_4$ photoanode was fabricated in the same way as described in section 2.2. To electrodeposit a BiOI layer on top of the $BiVO_4$ photoanode same procedure was followed as described in section 2.1. The only change was that the $BiVO_4$ photoanode replaced FTO as the working electrode in the three electrode electrochemical set-up. After the electrodeposition process, the $BiVO_4$/BiOI photoanode was washed with deionized water and after drying the $BiVO_4$/BiOI photoanode (shown in supplementary Fig. 2) was stored in a dry place under normal atmosphere for further use.

Fig. 1 in the supplementary information explains why 5 min was selected as the deposition time for the fabrication of the $BiVO_4$ photoanode and for the deposition of BiOI on the BiVO4 photoanode.

2.4. Structural and morphological characterization

Morphological and micro/nano-structure analysis of fabricated photoanodes was carried out by using field emission scanning electron microscopy (SEM) (FEI, Quanta F650) coupled with an Inca 250 SSD XMax20 detector for energy-dispersive X-ray spectrometer (EDS) analysis. The degree of crystallinity and purity of the photoanodes were determined with X-ray diffraction (XRD) using Cu Kα radiation within a range of 2 θ = 10°–130°, a step size of 0.040° 2 θ, and a counting time of 2 s per step. X-ray photoelectron spectroscopy (XPS) analysis was carried out with a Thermo Fisher K-Alpha surface analysis machine (Thermo Fisher Scientific, USA).

2.5. Optical and opto-electronic characterization

Optical properties of fabricated photoanodes were studied between 300 and 700 nm (5 nm step size) by using diffusive reflectance UV–vis spectroscopy (The LAMBDA 1050+ UV/Vis/NIR spectrophotometer, UV Winlab software). Incident photon-to-electron conversion efficiency (IPCE) was also measured between 280 and 700 nm by using a customized incident photon to current conversion efficiency (IPCE) set-up under 1 sun illumination (AM 1.5 standard conditions). Each IPCE measurement was carried out by using the $BiVO_4$/BiOI, $BiVO_4$ and BiOI photoanode each time as working electrode at 1 V (external bias) and a platinum wire as the counter electrode. 40 μg L^{-1} ACT dissolved in 0.1 M Na_2SO_4 solution was used as electrolyte for IPCE measurements. Linear sweep voltammetry (LSV) was carried out in a three electrode arrangement between −0.2 and 1.5 V (vs Ag/AgCl) at a scan rate of 100 mV s^{-1} in 0.1 M Na_2SO_4.

2.6. Photo-electrocatalytic (PEC) experiments

PEC based removal of ACT by using the prepared photoanodes was carried out by using Autolab potentiostat (PGSTAT128 N) in three electrode configuration set-up. A quartz reactor cell containing three electrodes and 167 mL of electrolyte solution was used for the PEC removal experiments. 0.1 M Na_2SO_4 containing 40 μg L^{-1} ACT having a pH of 6.8 was used as electrolyte for the removal experiments and demineralized water was used for the preparation of the electrolyte. Fabricated photoanodes, Ag/AgCl (3.0 M KCl) electrode and graphite plate (40 × 40 mm) were used as working electrode, reference electrode and counter electrode, respectively. A constant voltage of 1 V vs Ag/AgCl was applied during the removal experiment to minimize the rate of recombination in the fabricated photoanodes. Solar simulator SUNTEST XXL + having three air cooled 1700 W Xenon lamps emitting 1 sun

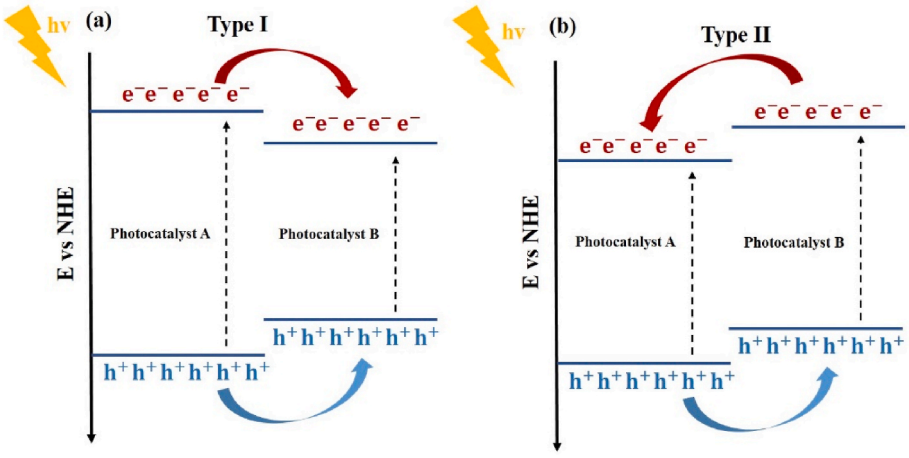

Fig. 1. Illustration showing the transfer of photogenerated holes and electrons in type I and type II heterojunction after the interaction of incoming solar photons with the $BiVO_4$ heterojunction photoanode.

illumination spectra was used as light source. The intensity of emitted light between 300 and 400 nm was calibrated to 60 W/m^2 and the distance between the light source and the photoanode was 13 cm. Each experiment ran for 5 h and samples were taken at an interval of 1 h for the analysis of ACT. Reusability experiments with $BiVO_4$/BiOI photoanode were performed by using same photoanode for three consecutive removal experiments of each 5 h experiment. Between successive experiments the photoanode was rinsed with demineralized water to remove any adsorbed acetaminophen on the photoanode.

2.6.1. Quenching experiments

Quenching experiments were carried out in a similar way as the removal experiments described in section 2.6, except the addition of quenching agents in the electrolyte. To quench the $^{\bullet}OH$ reactive species 5 mM methanol was added in the electrolyte because methanol has a high reaction rate constant of $9.7 \times 10^8\ M^{-1}s^{-1}$ with $^{\bullet}OH$ (Liang and Su, 2009), whereas in a separate experiment 5 mM p-BZQ (Orimolade and Arotiba, 2020c) was added in the electrolyte to quench $^{\bullet}O_2^-$. Each experiment ran for 5 h and samples were taken at an interval of 1 h for the quantification of ACT.

2.7. Analytical measurement of ACT

The concentration of ACT in the samples was measured by using liquid chromatography combined with tandem triple-quadrupole mass spectrometry (LC-MS). Acquity UPLC BEH C18 column from Waters was used in LC-MS to measure ACT in the samples. All Samples were first filtered with 0.2 μm glass fibre filters (GF-75, ADVANTEC®, Japan) and then 495 μL of filtered sample solution and 5 μL of internal standard (ACT-ring D4) calibration solution were added to the LC-MS sample vials. After mixing, the quantification of the target compound (ACT) in the samples was accomplished by the LC-MS device. Based on the concentration values of ACT, removal efficiency of each photoanode was calculated by using the following equation:

$$\text{Removal efficiency } (\%) = \left(\mathbf{1} - \frac{\boldsymbol{C_0}}{\boldsymbol{C_t}}\right) \times \mathbf{100}$$

where C_0 = Initial concentration at time t = 0 and C_t = Concentration at any time

3. Results and discussion

3.1. Structure and morphology of photoanodes

Fig. 2 shows the X-ray diffractograms of $BiVO_4$, BiOI and $BiVO_4$/BiOI photoanodes. In the case of $BiVO_4$, the characteristic peaks at 18.8°, 19.1°, 29.03°, 30.64°, 34.63°, 35.32°, 39.95°, 42.5°, 46.83°, 47.39°, 51.54°, 59.7° and 60.08° corresponded to monoclinic scheelite phase of $BiVO_4$ (JCPDS no. 75–1866). These characteristic peaks were in accordance with previous studies (Orimolade and Arotiba, 2020c; Orimolade et al., 2019a) indexed as (110), (011), (121), (040), (200), (002), (211), (015), (240), (042), (161), (321) and (123), respectively (Liu et al., 2018).Main peaks of BiOI at 30.01°, 32.19°, 45.89°, 51.95° and 55.65° are previously reported in literature (Xiao et al., 2018) and were indexed as (102), (110), (200), (114) and (212), respectively (Tang et al., 2019). The XRD pattern of $BiVO_4$/BiOI photoanode contains the characteristic peaks of both monoclinic scheelite $BiVO_4$ and BiOI (Ni et al., 2018), which confirms the successful deposition of BiOI on top of the $BiVO_4$ layer.

The scanning electron microscopy (SEM) images in Fig. 3 show the surface morphology of pristine $BiVO_4$ and heterojunction $BiVO_4$/BiOI photoanode. Fig. 3a shows homogenous distribution of $BiVO_4$ particles over FTO substrate after electrodeposition. The fabrication process proved to be effective in producing $BiVO_4$ particles of similar shape and size. Fig. 3b shows the magnified image of $BiVO_4$ particles that were

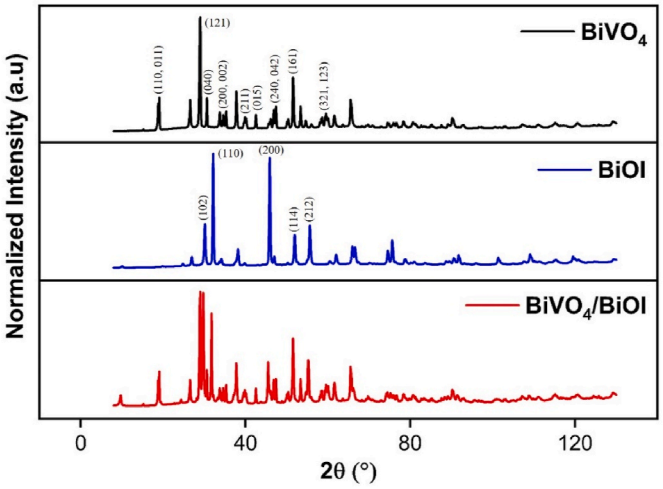

Fig. 2. XRD patterns of $BiVO_4$, BiOI and $BiVO_4$/BiOI photoanodes showing indexed characteristic peaks.

inter-connected to form a branched network. This branched network could facilitate an effective charge transfer at the interface of heterojunction. Fig. 3c shows the surface morphology of the $BiVO_4$/BiOI photoanode, which exhibited a homogeneous deposition of needle-like BiOI particles on top of the $BiVO_4$ layer. The magnified image in Fig. 3d shows the interaction of needle-like BiOI particles with the branched $BiVO_4$ particles. The interaction shows that there was an interfacial contact between the photocatalytic layers that will hold the potential to enhance the charge separation in the photoanode (McDonald and Choi, 2012). The energy dispersive X-Ray (EDX) spectrum shown in 3 (e) gives the compositional analysis of the heterojunction photoanode, and it consisted of only Bi, I, O and V. The element tin (Sn) in the EDX spectra came from the fluorine doped tin oxide (FTO) substrate. The EDX result also confirmed the purity of the deposited photocatalytic layers without any major impurity element present.

X-Ray photoelectron spectroscopy (XPS) survey results are shown in supplementary Fig. 3. The survey confirmed that only Bi, V, O, I, and C were present in the photoanodes and showed distinct peaks at their respective binding energies. The survey of $BiVO_4$/BiOI in particular confirmed the co-existence of Bi, V, O, I and C, which indicated the formation of a heterojunction. Carbon (C) is considered as impurity element and came from the atmosphere during the measurement. The de-convoluted high resolution spectra of elements (Bi, V, I, O) present in the photoanodes are also shown in Fig. 4. Starting with the Bi, two asymmetric peaks with different binding energies corresponded to two different spin orbit splitting states ($4f_{5/2}$ & $4f_{7/2}$) of Bi4f. The peaks at 162.85, 157.48 eV in $BiVO_4$ and 163.98, 158.58 eV in BiOI were related to $Bi4f_{5/2}$ and $Bi4f_{7/2}$ respectively (Meng et al., 2020; Ni et al., 2018, p. 4). These characteristic peaks of Bi4f also suggest that Bi was present in the form of Bi^{3+} in the crystal lattice. The peak positions of $Bi4f_{5/2}$ and $Bi4f_{7/2}$ in $BiVO_4$/BiOI photoanode were at 163.58 and 158.28 eV, respectively. The slight increase in binding energies of Bi4f in $BiVO_4$/-BiOI photoanode compared to pristine $BiVO_4$ could be due to a loss of surface bound oxygen and hydroxyl groups, which decreased the electron concentration around Bi (Ni et al., 2018, p. 4). Vanadium was also present in two different spin orbital states as $V2p_{1/2}$ and $V2p_{3/2}$ in both $BiVO_4$ and $BiVO_4$/BiOI photoanode. Two distinct peaks at 528.28 and 515.08 eV corresponded to $V2p_{1/2}$ and $V2p_{3/2}$ in $BiVO_4$, whereas the peaks at 529.08 and 515.98 eV were related to $V2p_{1/2}$ and $V2p_{3/2}$ in $BiVO_4$/BiOI photoanode. The peak positions of $V2p_{1/2}$ and $V2p_{3/2}$ suggest that V was present as V^{5+} in both photoanodes (Zhang et al., 2019; Fang et al., 2017). Two relatively sharp peaks at 629.98 and 618.48 eV are attributed to $I3d_{3/2}$ and $I3d_{5/2}$ in BiOI electrode. The peaks at 629.68 and 618.18 eV corresponded to $I3d_{3/2}$ and $I3d_{5/2}$, respectively, in the

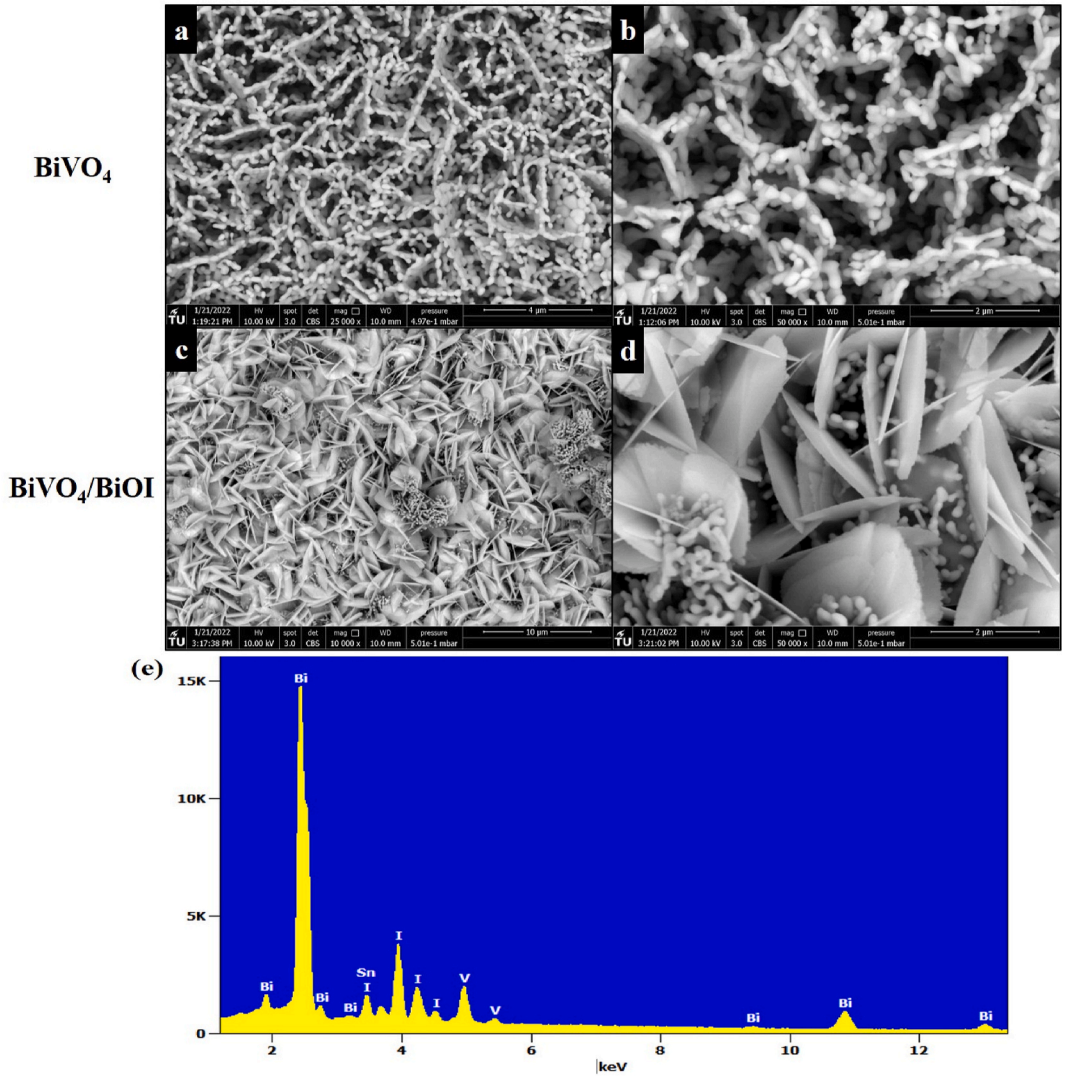

Fig. 3. SEM surface morphology images of $BiVO_4$ (a) (b), $BiVO_4$/BiOI (c) (d) and EDX spectra of $BiVO_4$/BiOI showing the peaks of elements present in the photoanode (e).

$BiVO_4$/BiOI photoanode. The peak positions of I3d in both photoanodes indicated that I was present in −1 oxidation state in the lattice structure (Hou et al., 2017). Furthermore, there was no significant shift in the binding energies of $I3d_{3/2}$ and $I3d_{5/2}$ in $BiVO_4$/BiOI photoanode compared to BiOI, confirming that the chemical environment around I was the same in both photoanodes. In $BIVO_4$, O1s peaks observed at 528.18 and 528.98 eV corresponded to lattice oxygen bonded to Bi and V, respectively, whereas a diminishing peak at 530.8 eV was attributed to surface adsorbed O–OH molecules. In case of BiOI, the strong peak observed at 529.38 eV was related to lattice oxygen bonded to Bi, and a small peak at 530.88 eV that was also observed in $BiVO_4$ corresponded to surface absorbed O–OH molecules (Ni et al., 2018). In the heterojunction photoanode, the O1s peak at 529.08 eV corresponded to lattice oxygen whereas the peak at 530.28 eV was attributed to surface adsorbed O–OH molecules. Because the binding energy of O1s in heterojunction photoanode was closer to the binding energy of the BiOI O1s peak, it can be inferred that the Bi–O interaction was stronger in heterojunction photoanode than pristine $BiVO_4$ photoanode. Overall, the XPS results show that both $BiVO_4$ and BiOI co-existed in heterojunction photoanode, which was in accordance with the XRD and SEM results.

3.2. Optical and opto-electronic properties of prepared photoanodes

UV–Vis diffusive reflectance spectroscopy was used to analyse the optical properties of the fabricated photoanodes. Fig. 5a shows the absorbance pattern of $BiVO_4$, BiOI and $BiVO_4$/BiOI photoanodes and it is evident from Fig. 5a that all three photoanodes absorbed in the UV–Visible range. As BiOI absorbed strongly in the visible range, combining it with $BiVO_4$ gave an increase in the absorbance edge of heterojunction photoanode as is shown in Fig. 5a. The absorbance edges of $BiVO_4$, BiOI and $BiVO_4$/BiOI photoanodes were around 501, 636 and 647 nm, respectively. The absorbance results confirmed that combining $BiVO_4$ and BiOI increased the absorbance range of the heterojunction photoanode. Furthermore, the absorbance data was used to estimate the band gap energies of the $BiVO_4$ and BiOI photoanodes using the Tauc equation as given below: (Huang et al., 2018).

$$\alpha h\nu = A\left(\nu h - E_g\right)^{n/2} \quad (1)$$

where α, h, ν, A and E_g correspond to absorbance coefficient, Planck's constant, incident light frequency, constant and band gap energy, respectively in Eq. (1). The exponent n is a constant whose value is dependent on the optical transition behaviour of the photocatalyst under consideration. The value of n for a direct transition semiconductor such

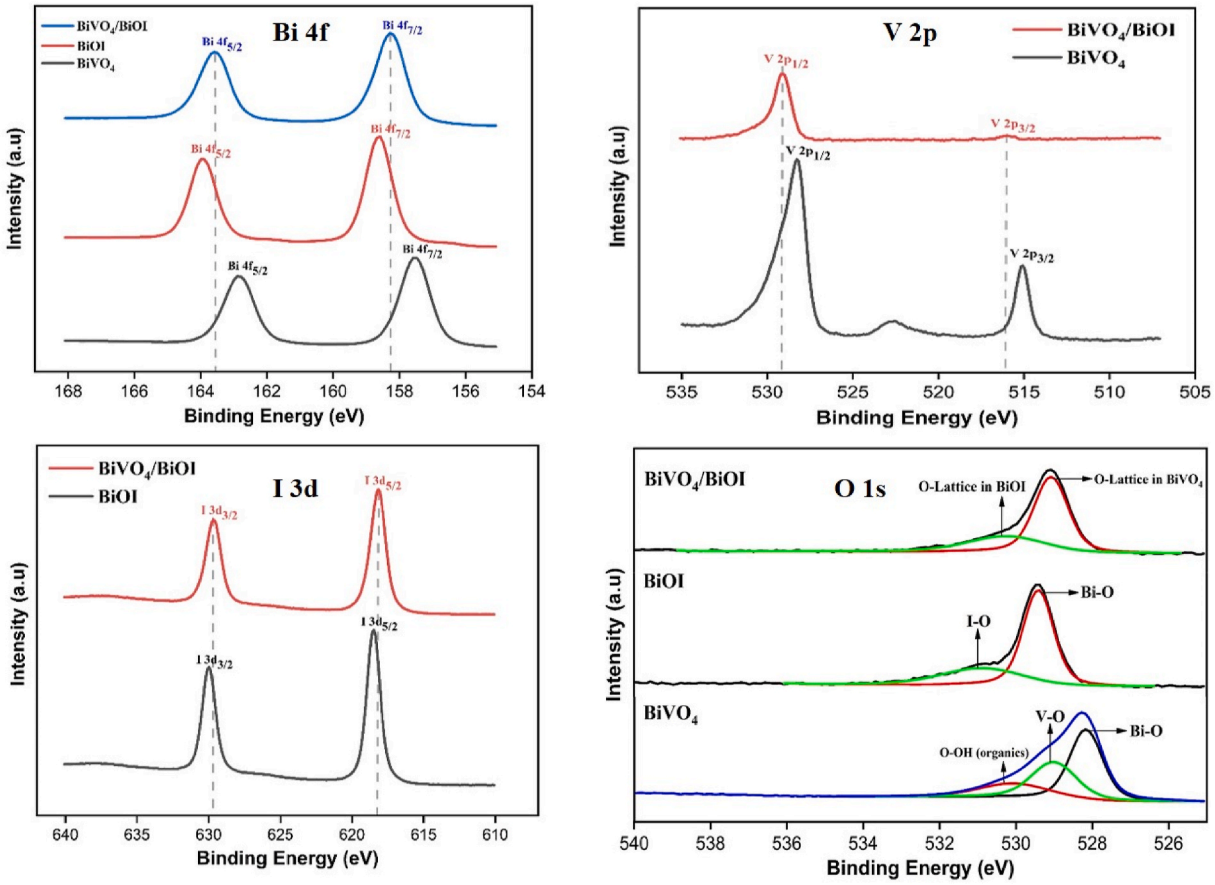

Fig. 4. De-convoluted and high resolution elemental XPS spectra of Bi4f, V2p, I3d and O1s showing different orbital states, bonding environment and their respective binding energies.

as $BiVO_4$ is 1 (Ju et al., 2016). Therefore, a plot of $(\alpha h\nu)^2$ versus photon energy (hv) was made as shown in supplementary Fig. 4 to estimate the band gap energy, which was 2.49 eV. Similarly, BiOI is an indirect optical transition semiconductor whose n value is 4 (Xiang et al., 2016). After substituting the value of n = 4 in the Tauc equation a plot between $(\alpha h\nu)^{1/2}$ versus photon energy (hv) is made from which a band gap energy of 1.80 eV was obtained. The calculated values of band gap energies for $BiVO_4$ and BiOI photoanodes were very close to previously reported values in the literature (Xiang et al., 2016; Orimolade et al., 2019a). UV–vis absorbance results clearly showed that the absorbance region of $BiVO_4$/BiOI photoanode was broader compared to $BiVO_4$ and BiOI, which confirmed the successful formation of a heterojunction.

Calculated band gap energies (E_g) were used to calculate the valence band (E_{VB}) and conduction band (E_{CB}) potentials of $BiVO_4$ and BiOI. Following equations were used to calculate E_{VB} and E_{CB} (Orimolade et al., 2019a, p. 4).

$$E_{CB} = X - E_C - 0.5E_g \quad (2)$$

$$E_{VB} = E_g + E_{CB} \quad (3)$$

wherein X is the geometric mean of the absolute electronegativities of all the constituent atoms present in the photocatalyst. The value of X for $BiVO_4$ is 6.04 eV, whereas for BiOI it is 6.10 eV (Pearson, 1988). E_c corresponds to the energy of free electrons with respect to hydrogen scale (NHE) and its value is 4.50 eV. E_g corresponds to the band gap energies of the respective photoanodes that were calculated using Tauc plots. By substituting the values of X, E_c and E_g in the above equations, the band edge potentials of $BiVO_4$ and BiOI were calculated. For BiOI the values of E_{CB} and E_{VB} were 0.7 and 2.5 eV, respectively, whereas for $BiVO_4$ the values of E_{CB} and E_{VB} were 0.29 and 2.78 eV, respectively. These band edge potential values show that the heterojunction that was formed between $BiVO_4$ and BiOI was of type I. In type I heterojunction both photogenerated charge carriers are transferred to the electrode-electrolyte interface (Orimolade and Arotiba, 2020b) as shown in Fig. 5b. One intrinsic drawback of type I heterojunction is that there is a high chance of recombination if the photogenerated charge carriers are not consumed at the electrode electrolyte interface (Orimolade and Arotiba, 2020b). Application of a positive bias (applied potential >0) in type I heterojunction enhances the charge separation efficiency by creating an electric field at the heterojunction that pulls apart electrons and holes (Orimolade and Arotiba, 2020a; Li et al., 2022). Furthermore, in PEC based water treatment processes, the photogenerated holes and electrons are used to produce $^{\bullet}OH$ and $^{\bullet}O_2^-$ radicals which oxidize the organic pollutants (Orimolade and Arotiba, 2020c). Therefore, chances of recombination are reduced if photogenerated holes and electrons are consumed for the generation of $^{\bullet}OH$ and $^{\bullet}O_2^-$.

Linear sweep voltammetry (LSV) was carried out to study the effect of applying external voltage on the photocurrent generated by the photoanodes. In Fig. 5c, as expected the photocurrent generated by $BiVO_4$/BiOI photoanode in the presence of simulated solar light was higher compared to pristine $BiVO_4$ and BiOI. In illuminated conditions, the increase in the application of external voltage yielded a positive impact on the photo-current of all three types of photoanodes, confirming that the application of external bias reduced the rate of recombination. 1.0 V was chosen as the optimum potential to be applied for the PEC removal of ACT because at this potential sufficient current was generated. Increase in photocurrent of $BiVO_4$/BiOI photoanode implied that more charges (electrons and holes) were available at the electrode-electrolyte interface for the generation of reactive oxygen

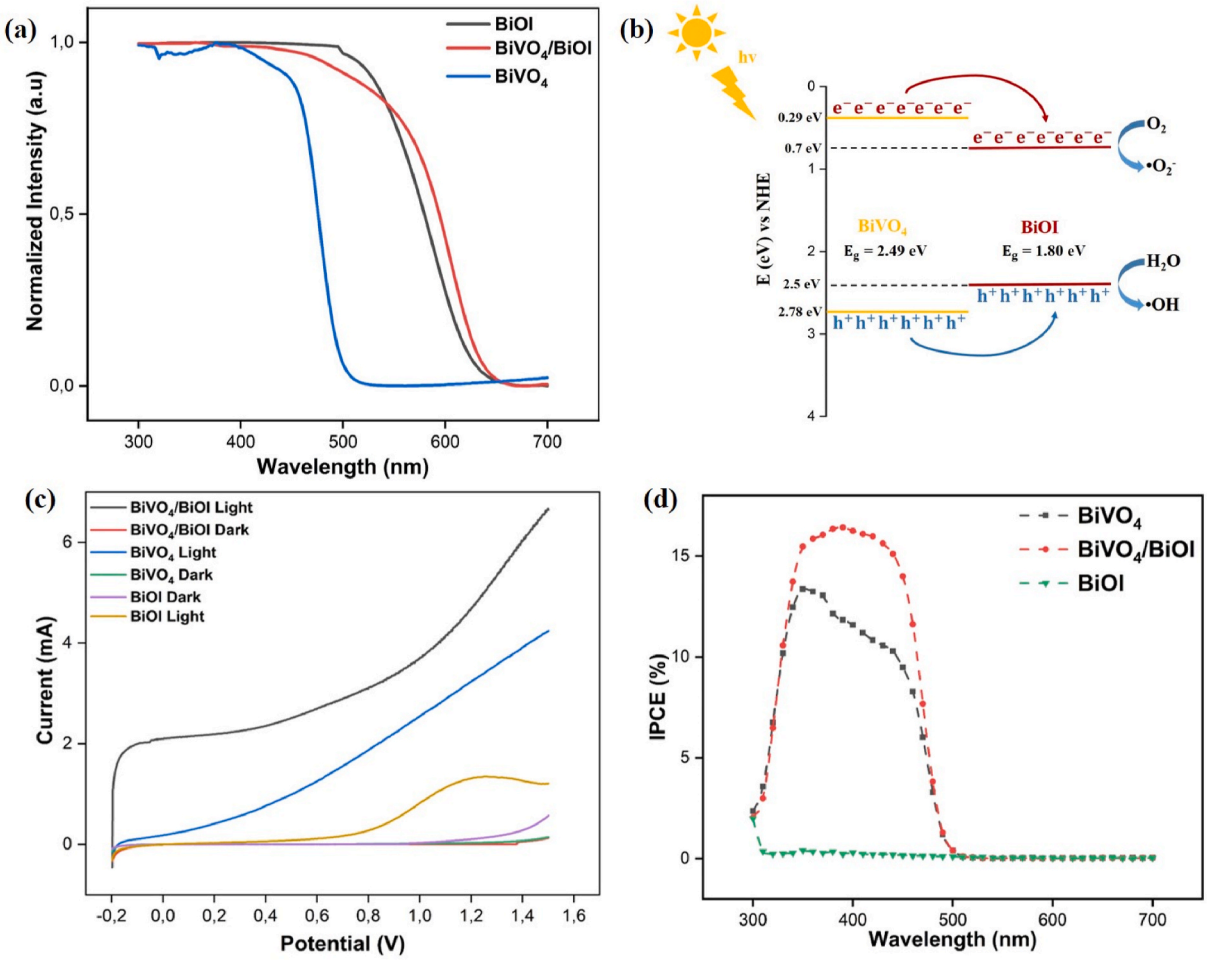

Fig. 5. (a) UV–Visible diffusive reflectance spectra of $BiVO_4$, BiOI and $BiVO_4$/BiOI photoanodes showing the absorbance range (b) Illustration of photogenerated holes and electrons for the generation of $^{\bullet}OH$ and $^{\bullet}O_2^-$ radicals after the interaction of solar photons with $BiVO_4$/BiOI photoanode (c) LSV curves for $BiVO_4$, BiOI and $BiVO_4$/BiOI photoanodes under dark and illuminated conditions performed from −0.2 to 1.5 V at 100 mV s^{-1} scan rate (d) IPCE plots for $BiVO_4$, BiOI and $BiVO_4$/BiOI photoanodes under 1 sun illumination at 1 V external bias vs platinum wire as counter electrode.

species (ROS). As a result, the formation of heterojunction will increase the removal kinetics of ACT in demineralized water because of the increased in-situ generation of $^{\bullet}OH$ and $^{\bullet}O_2^-$. There is negligible current in the absence of light (dark), which means that applying an external voltage to the photoanodes in the absence of light will be of no use for the removal of ACT.

Incident photon to current conversion efficiency (IPCE) measurements were performed to study the quantum efficiency of fabricated photoanodes. Quantum efficiency measures the amount of electrons generated in response to the incident photons absorbed by the photoanode. Fig. 5d shows the IPCE plots of BiOI, $BiVO_4$ and BiVO4/BiOI photoanodes. Fig. 5d clearly shows that $BiVO_4$ and heterojunction photoanode exhibits high incident photon to current conversion efficiency in UV–visible range. In case of $BiVO_4$, the maximum IPCE yield was 13% and it occurred at 350 nm (λ_{max}), whereas after the formation of heterojunction the maximum IPCE yield increased to 16% at λ_{max} = 390 nm. Pristine BiOI photoanode showed negligible IPCE yield which corresponded to its intrinsic high rate of recombination. Overall, the IPCE result illustrates that the formation of heterojunction not only increased the incident photon to current conversion efficiency by 23% but it also shifted the λ_{max} further in the visible region. The IPCE measurement also gives the value of short circuit photo-current (J_{sc}), which corresponds to the maximum current that can be drawn from the photoanode (Gong et al., 2016). The $BiVO_4$ photoanode yielded a J_{sc} of 4.88 A m^{-2}, whereas $BiVO_4$/BiOI photoanode yielded a J_{sc} of 7.05 A/m^2. This increase in IPCE and J_{sc} values as compared to $BiVO_4$ and BiOI was attributed to the interface of $BiVO_4$ and BiOI photocatalyts that increased the charge separation efficiency and thus reduced the rate of recombination in the heterojunction photoanode.

3.3. Photoelectrocatalytic removal of ACT

Fig. 6a shows the normalized decrease in concentration of ACT in demineralized water by using $BiVO_4$, BiOI and $BiVO_4$/BiOI photoanodes at an applied external voltage of 1 V vs Ag/AgCl (reference electrode). Direct irradiation with simulated sunlight from the solar simulator (photolysis) of the ACT solution had limited effect as it only removed 7% ACT in 5 h. PEC based removal of ACT by using BiOI photoanode showed 24% removal in 5 h. Fig. 6a shows that formation of heterojunction had a positive impact on the ACT removal. Although both $BiVO_4$ and $BiVO_4$/BiOI removed 100% ACT after 5 h, the evolution of the removal efficiency is different. Fig. 6b provides more detailed insight on the removal efficiency of ACT on hourly basis. Fig. 6b shows that $BiVO_4$/BiOI photoanode removed more than half of the ACT within the first hour, which was a 22% increase in removal efficiency compared to $BiVO_4$. This increasing trend in the removal efficiency continued till 2 h and after that the removal efficiency of both photoanodes were similar. It can be observed in Fig. 6b that the removal efficiency increased with time, however, its rate of increment decreased with time. This was explained by the decrease in ACT concentration in the bulk solution, therefore, the

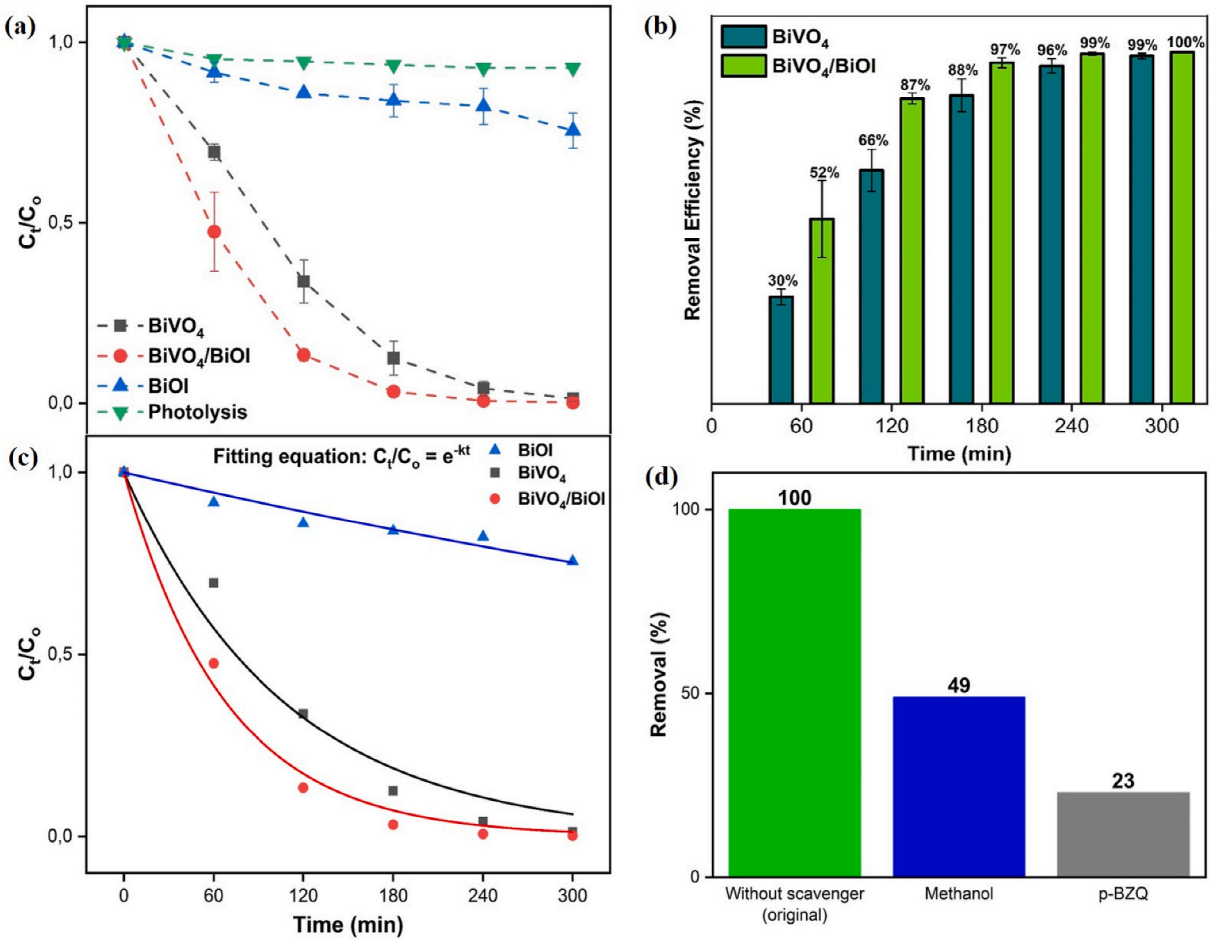

Fig. 6. (a) Normalized decrease in concentration of ACT during 5 h of removal experiment by using the fabricated photoanodes at an external bias of 1 V vs Ag/AgCl (b) Comparison of removal efficiency of $BiVO_4$ and $BiVO_4$/BiOI photoanode on hourly basis (c) Determination of first order rate coefficients of $BiVO_4$, BiOI and $BiVO_4$/BiOI photoanodes during 5 h of removal experiments (d) Removal efficiency of $BiVO_4$/BiOI photoanode in the presence of quenching agent. 5 mM methanol was used to quench $^{\bullet}OH$ radicals and 5 mM p-BZQ was used to quench $^{\bullet}O_2^-$ radicals.

reaction became partially diffusion controlled in which the diffusion of ACT molecules from bulk towards the surface of the photoanode became slower. The diffusion of ACT molecules to the surface is important because the oxidation reaction takes place within the vicinity of photoanode-electrolyte interface due to the short lifetime of ROS ($^{\bullet}OH$ and $^{\bullet}O_2^-$ radicals) (Attri et al., 2015). According to previous studies related to ACT degradation suggest that three initial oxidation/hydroxylation reactions compete with each other (Vogna et al., 2002; Moctezuma et al., 2012). In these reactions the reactive species ($^{\bullet}OH$ and $^{\bullet}O_2^-$ radicals) attack the aromatic ring of ACT to form ortho-, para- or meta-hydroxylation products of ACT (Vogna et al., 2002). Nuclear magnetic resonance (NMR) studies have shown that the meta-position is relatively favourable for further degradation of ACT (Moctezuma et al., 2012), however, the complete mechanism of ACT degradation cannot be proposed in this study because the intermediates/transformation products of ACT were not analysed.

Kinetic plots for $BiVO_4$, BiOI $BiVO_4$/BiOI are shown in Fig. 6c. Because the normalized removal followed a classical first order reaction, first order rate equation ($C/C_0 = e^{-k/t}$) was used to determine the rate coefficients of $BiVO_4$, BiOI and $BiVO_4$/BiOI photoanodes. As expected, the rate coefficient of $BiVO_4$/BiOI photoanode (shown in Table 1) compared to $BiVO_4$ is 57% higher. The overall superior performance of $BiVO_4$/BiOI in removing ACT from demineralized water is attributed to the formation of heterojunction that facilitated the charge separation efficiency. Similarly, the applied external voltage of 1 V (vs Ag/AgCl) further decreased the rate of recombination by diverting the electrons from the conduction band to the external electrical circuit.

The removal rate coefficient of the $BiVO_4$/BiOI photoanode given in Table 1 is similar or higher than the rate coefficients reported in literature that applied $BiVO_4$ based photoanodes for the removal of different pharmaceuticals such as phenol (20 mg L^{-1}; $k = 0.5 \times 10^{-2}$ min^{-1}) (Bennani et al., 2016), bisphenol A (10 mg L^{-1}; $k = 4.1 \times 10^{-2}$ min^{-1}) (Shao et al., 2020b), norfloxacin (10 mg L^{-1}; $k = 0.268 \times 10^{-2}$ min^{-1}) (Du et al., 2019, p. 3), tetracycline hydrochloride (10 mg L^{-1}; $k = 0.51 \times 10^{-2}$ min^{-1}) (Lu et al., 2019) and dyes such as methyl orange (10 mg L^{-1}; $k = 2.9 \times 10^{-2}$ min^{-1}) (Bacha et al., 2019) and rhodamine B (10 mg L^{-1}; $k = 0.92 \times 10^{-2}$ min^{-1}) (Orimolade et al., 2019b). Although, these studies report first order removal kinetics and the pollutant concentrations vary between 8 and 20 mg L^{-1}, the reported rate coefficients are not drastically higher than those of the $BiVO_4$/BiOI photoanode given in Table 1. In terms of applied external potential (electrical energy input) most studies used between 1 and 2 V vs Ag/AgCl as an external bias for an average reaction time of around 2.5 h with approximately 80%

Table 1
First order rate coefficients of BiOI, $BiVO_4$ and $BiVO_4$/BiOI photoanodes after 5 h of illumination.

Photoanode	Rate coefficient (min^{-1})	R^2
BiOI	9.50×10^{-4}	0.928
$BiVO_4$	9.32×10^{-3}	0.967
$BiVO_4$/BiOI	1.46×10^{-2}	0.928

removal of organic compounds from aqueous solution (Bennani et al., 2016; Bacha et al., 2019; Orimolade et al., 2020; Orimolade and Arotiba, 2020c; Wang et al., 2020). In this study PEC based ACT removal showed faster removal kinetics than in most of the studies reported in literature with a similar electrical energy input.

Quenching studies are normally performed to gain information about the main oxidants involved in the removal reaction of organic pollutants (Orimolade and Arotiba, 2020c). According to previous studies (Orimolade and Arotiba, 2020c), hydroxyl radicals ($^{\bullet}OH$) and super oxide radicals ($^{\bullet}O_2^-$) are the two main oxidising species responsible for the removal of organic micro-pollutants. Quenching experiments were carried out for $BiVO_4$/BiOI photoanode by using methanol and p-benzoquinone (p-BZQ) to quench $^{\bullet}OH$ and $^{\bullet}O_2^-$, respectively, in the reaction solution of ACT. The results of the quenching experiments after 5 h of illumination are shown in Fig. 6d. The figure shows that the removal efficiency of $BiVO_4$/BiOI photoanode in the presence of both quenching agents was lower than without quenching agents, which confirmed the effect of $^{\bullet}OH$ and $^{\bullet}O_2^-$ radicals on the removal of ACT.

Removal in the presence of methanol was higher than in the presence of p-BZQ, which indicates that the $^{\bullet}O_2^-$ was the main reactive specie in our research, because the $BiVO_4$/BiOI photoanode only removed 23% ACT in the presence of p-BZQ. Overall, the results of the quenching study suggest that both $^{\bullet}OH$ and $^{\bullet}O_2^-$ were responsible for the ACT removal as the removal efficiency also decreased in the presence of methanol. This joint attack of both reactive species was due to the formation of type I heterojunction as mentioned in section 3.2, where both reactive species ($^{\bullet}OH$ and $^{\bullet}O_2^-$) were generated within the vicinity of photoanode surface. The finding of the quenching study is in accordance with the literature where researchers have reported different photocatalysts for the in-situ oxidation of organic compounds and dyes through $^{\bullet}O_2^-$ as the main oxidant (Li et al., 2011; Byzynski et al., 2018). The results of reusability experiments are shown in the supplementary information. Fig. 5 in the supplementary information shows the removal efficiency of a $BiVO_4$/BiOI photoanode that was used for 3 consecutive removal experiments of each 5 h. The removal efficiency after the third run dropped down from 100% to 74%, meaning a decrease of 26% after 15 h of using the same photoanode. This drop in efficiency could be because of the adsorption of ACT molecules within the surface pores of $BiVO_4$/BiOI photoanode that reduced the available surface area for the ROS generation.

In summary, the formation of heterojunction enhanced the kinetics of the ACT removal as shown in Fig. 6c and this enhancement was attributed to type I heterojunction that generated both $^{\bullet}OH$ and $^{\bullet}O_2^-$ radicals at the photoanode-electrolyte interface. The generated $^{\bullet}OH$ and $^{\bullet}O_2^-$ radicals unselectively attacked the molecules of ACT to remove them from the electrolyte.

4. Conclusions

Successful fabrication of $BiVO_4$, BiOI and $BiVO_4$/BiOI photoanodes was achieved by using electrodeposition. Fabricated photoanodes were characterized by using structural, morphological, optical and opto-electronic characterization techniques. Successful and effective formation of $BiVO_4$/BiOI heterojunction was confirmed with diffusive reflectance UV–Vis spectroscopy and IPCE characterization. Band edge potential calculations showed that a type I heterojunction was formed that enhanced the kinetics of ACT removal in demineralized water. BiOI, $BiVO_4$ and $BiVO_4$/BiOI photoanodes showed removal efficiency of 24, 99 and 100%, respectively. Although the removal efficiency of $BiVO_4$ and $BiVO_4$/BiOI after 5 h were almost the same, the first order rate coefficient of $BiVO_4$/BiOI photoanode showed a 57% higher value as compared to $BiVO_4$ photoanode. Furthermore, the quenching study demonstrated that $^{\bullet}O_2^-$ radicals were the main reactive species in the removal of ACT. In conclusion, our research demonstrated the successful formation of $BiVO_4$/BiOI heterojunction photoanode that enhanced the removal kinetics of ACT (40 μg L^{-1}) in demineralized water compared to $BiVO_4$ and BiOI photoanodes.

Author contributions statement

Agha Zeeshan Ali: Conceptualization, Methodology, Validation, Formal Analysis, Writing – original draft, Writing – review & editing, Visualization, Project administration, **Yiqian Wu:** Investigation, Validation, Data curation, **Yasmina-Doekhi Bennani:** Supervision, Writing – review & editing, **Henri Spanjers:** Supervision, Writing – review & editing, Funding acquisition, **Jan Peter van der Hoek:** Supervision, Writing – review & editing, Funding acquisition.

Declaration of competing interest

The authors declare that they have no known competing financial interests or personal relationships that could have appeared to influence the work reported in this paper.

Data availability

Data will be made available on request.

Acknowledgement

This research study was part of InnovEOX project that has received funding from the European Union's EU Framework Programme for Research and Innovation Horizon 2020 under Grant Agreement No 861369.

Appendix A. Supplementary data

Supplementary data to this article can be found online at https://doi.org/10.1016/j.chemosphere.2023.138322.

References

Aragaw, T.A., Bogale, F.M., Aragaw, B.A., 2021. Iron-based nanoparticles in wastewater treatment: a review on synthesis methods, applications, and removal mechanisms. J. Saudi Chem. Soc. 25, 101280 https://doi.org/10.1016/j.jscs.2021.101280.

Attri, P., Kim, Y.H., Park, D.H., Park, J.H., Hong, Y.J., Uhm, H.S., Kim, K.-N., Fridman, A., Choi, E.H., 2015. Generation mechanism of hydroxyl radical species and its lifetime prediction during the plasma-initiated ultraviolet (UV) photolysis. Sci. Rep. 5, 9332. https://doi.org/10.1038/srep09332.

Bacha, A.-U.-R., Cheng, H., Han, J., Nabi, I., Li, K., Wang, T., Yang, Y., Ajmal, S., Liu, Y., Zhang, L., 2019. Significantly accelerated PEC degradation of organic pollutant with addition of sulfite and mechanism study. Appl. Catal. B Environ. 248, 441–449. https://doi.org/10.1016/j.apcatb.2019.02.049.

Bai, S., Liu, J., Cui, M., Luo, R., He, J., Chen, A., 2018. Two-step electrodeposition to fabricate the p–n heterojunction of a $Cu_2O/BiVO_4$ photoanode for the enhancement of photoelectrochemical water splitting. Dalton Trans. 47, 6763–6771. https://doi.org/10.1039/C7DT04258B.

Bennani, Y., Perez-Rodriguez, P., Alani, M.J., Smith, W.A., Rietveld, L.C., Zeman, M., Smets, A.H.M., 2016. Photoelectrocatalytic oxidation of phenol for water treatment using a $BiVO_4$ thin-film photoanode. J. Mater. Res. 31, 2627–2639. https://doi.org/10.1557/jmr.2016.290.

Byzynski, G., Volanti, D.P., Ribeiro, C., Mastelaro, V.R., Longo, E., 2018. Direct photo-oxidation and superoxide radical as major responsible for dye photodegradation mechanism promoted by TiO_2–rGO heterostructure. J. Mater. Sci. Mater. Electron. 29, 17022–17037. https://doi.org/10.1007/s10854-018-9799-0.

Cao, D., Wang, Y., Qiao, M., Zhao, X., 2018. Enhanced photoelectrocatalytic degradation of norfloxacin by an $Ag_3PO_4/BiVO_4$ electrode with low bias. J. Catal. 360, 240–249. https://doi.org/10.1016/j.jcat.2018.01.017.

Chowdhury, A., Sajid, M., Jahan, N., Adelusi, T.I., Maitra, P., Yin, G., Wu, X., Gao, Y., Wang, S., 2021. A secondary approach with conventional medicines and supplements to recuperate current COVID-19 status. Biomed. Pharmacother. 142, 111956 https://doi.org/10.1016/j.biopha.2021.111956.

Collivignarelli, M.C., Abbà, A., Carnevale Miino, M., Bertanza, G., Sorlini, S., Damiani, S., Arab, H., Bestetti, M., Franz, S., 2021. Photoelectrocatalysis on TiO_2 meshes: different applications in the integrated urban water management. Environ. Sci. Pollut. Res. 28, 59452–59461. https://doi.org/10.1007/s11356-021-12606-5.

Corominas, L., Acuña, V., Ginebreda, A., Poch, M., 2013. Integration of freshwater environmental policies and wastewater treatment plant management. Sci. Total Environ. 445, 185–191. https://doi.org/10.1016/j.scitotenv.2012.12.055. –446.

Deshpande, N.G., Ahn, C.H., Koli, R.R., Jamadar, A.S., Kim, D.S., Kim, Y.B., Jung, S.H., Cho, H.K., 2020. Controlled nanostructured morphology of $BiVO_4$ photoanodes for efficient on-demand catalysis in solar water-splitting and sustainable water-treatment. Appl. Surf. Sci. 514, 146075 https://doi.org/10.1016/j.apsusc.2020.146075.

Du, H., Pu, W., Wang, Y., Yan, K., Feng, J., Zhang, J., Yang, C., Gong, J., 2019. Synthesis of $BiVO_4/WO_3$ composite film for highly efficient visible light induced photoelectrocatalytic oxidation of norfloxacin. J. Alloys Compd. 787, 284–294. https://doi.org/10.1016/j.jallcom.2019.01.390.

Fang, D., Li, X., Liu, H., Xu, W., Jiang, M., Li, W., Fan, X., 2017. $BiVO_4$-rGO with a novel structure on steel fabric used as high-performance photocatalysts. Sci. Rep. 7, 7979. https://doi.org/10.1038/s41598-017-07342-1.

Garcia-Segura, S., Brillas, E., 2017. Applied photoelectrocatalysis on the degradation of organic pollutants in wastewaters. J. Photochem. Photobiol. C Photochem. Rev. 31, 1–35. https://doi.org/10.1016/j.jphotochemrev.2017.01.005.

Golovko, O., Rehrl, A.-L., Köhler, S., Ahrens, L., 2020. Organic micropollutants in water and sediment from lake mälaren, Sweden. Chemosphere 258, 127293. https://doi.org/10.1016/j.chemosphere.2020.127293.

Gong, H., Freudenberg, N., Nie, M., van de Krol, R., Ellmer, K., 2016. $BiVO_4$ photoanodes for water splitting with high injection efficiency, deposited by reactive magnetron co-sputtering. AIP Adv. 6, 045108 https://doi.org/10.1063/1.4947121.

He, T., Wu, D., Tan, Y., 2016. Fabrication of $BiOI/BiVO_4$ heterojunction with efficient visible-light-induced photocatalytic activity. Mater. Lett. 165, 227–230. https://doi.org/10.1016/j.matlet.2015.12.002.

Hou, J., Jiang, K., Shen, M., Wei, R., Wu, X., Idrees, F., Cao, C., 2017. Micro and nano hierachical structures of BiOI/activated carbon for efficient visible-light-photocatalytic reactions. Sci. Rep. 7, 11665 https://doi.org/10.1038/s41598-017-12266-x.

Huang, H., Ma, C., Zhu, Z., Yao, X., Liu, Y., Liu, Z., Li, C., Yan, Y., 2018. Insights into enhanced visible light photocatalytic activity of t-Se nanorods/BiOCl ultrathin nanosheets 1D/2D heterojunctions. J. Chem. Eng. 338, 218–229. https://doi.org/10.1016/j.cej.2017.12.012.

Ju, P., Wang, Y., Sun, Y., Zhang, D., 2016. Controllable one-pot synthesis of a nest-like $Bi_2WO_6/BiVO_4$ composite with enhanced photocatalytic antifouling performance under visible light irradiation. Dalton Trans. 45, 4588–4602. https://doi.org/10.1039/C6DT00118A.

Kim, T.W., Choi, K.-S., 2014. Nanoporous $BiVO_4$ photoanodes with dual-layer oxygen evolution catalysts for solar water splitting. Science 343, 990–994. https://doi.org/10.1126/science.1246913.

Lee, W.J., Goh, P.S., Lau, W.J., Ismail, A.F., 2020. Removal of pharmaceutical contaminants from aqueous medium: a state-of-the-art review based on paracetamol. Arabian J. Sci. Eng. 45, 7109–7135. https://doi.org/10.1007/s13369-020-04446-1.

Li, L.-P., Liu, M., Zhang, W.-D., 2018. Electrodeposition of CdS onto $BiVO_4$ films with high photoelectrochemical performance. J. Solid State Electrochem. 22, 2569–2577. https://doi.org/10.1007/s10008-018-3973-4.

Li, S., Xu, W., Meng, L., Tian, W., Li, L., 2022. Recent progress on semiconductor heterojunction-based photoanodes for photoelectrochemical water splitting. Small Sci. 2, 2100112 https://doi.org/10.1002/smsc.202100112.

Li, Y., Niu, J., Yin, L., Wang, W., Bao, Y., Chen, J., Duan, Y., 2011. Photocatalytic degradation kinetics and mechanism of pentachlorophenol based on Superoxide radicals. J. Environ. Sci. 23, 1911–1918. https://doi.org/10.1016/S1001-0742(10)60563-3.

Liang, C., Su, H.-W., 2009. Identification of sulfate and hydroxyl radicals in thermally activated persulfate. Ind. Eng. Chem. Res. 48, 5558–5562. https://doi.org/10.1021/ie9002848.

Liao, M., Su, L., Deng, Y., Xiong, S., Tang, R., Wu, Z., Ding, C., Yang, L., Gong, D., 2021. Strategies to improve WO_3-based photocatalysts for wastewater treatment: a review. J. Mater. Sci. 56, 14416–14447. https://doi.org/10.1007/s10853-021-06202-8.

Liu, Y., Li, H., Zhang, X., Liu, S., Zhang, Y., Li, Q., Liu, J., 2018. PEG-assisted hydrothermal synthesis of novel flower-like hierarchical $BiVO_4$ with enhanced visible light photocatalytic activity. IOP Conf. Ser. Mater. Sci. Eng. 452, 042105 https://doi.org/10.1088/1757-899X/452/4/042105.

López Zavala, M.Á., Vega, D.A., Álvarez Vega, J.M., Castillo Jerez, O.F., Cantú Hernández, R.A., 2020. Electrochemical oxidation of acetaminophen and its transformation products in surface water: effect of pH and current density. Heliyon 6, e03394. https://doi.org/10.1016/j.heliyon.2020.e03394.

Lu, Y., Chu, Y., Zheng, W., Huo, M., Huo, H., Qu, J., Yu, H., Zhao, Y., 2019. Significant tetracycline hydrochloride degradation and electricity generation in a visible-light-driven dual photoelectrode photocatalytic fuel cell using $BiVO_4/TiO_2$ NT photoanode and Cu_2O/TiO_2 NT photocathode. Electrochim. Acta 320, 134617. https://doi.org/10.1016/j.electacta.2019.134617.

McDonald, K.J., Choi, K.-S., 2012. A new electrochemical synthesis route for a BiOI electrode and its conversion to a highly efficient porous $BiVO_4$ photoanode for solar water oxidation. Energy Environ. Sci. 5, 8553–8557. https://doi.org/10.1039/C2EE22608A.

Meng, S., Ogawa, T., Okumura, H., Ishihara, K.N., 2020. Enhanced photocatalytic activity of $BiVO_4/Bi_2S_3/SnS_2$ heterojunction under visible light. Catalysts 10, 1294. https://doi.org/10.3390/catal10111294.

Moctezuma, E., Leyva, E., Aguilar, C.A., Luna, R.A., Montalvo, C., 2012. Photocatalytic degradation of paracetamol: intermediates and total reaction mechanism. J. Hazard Mater. 243, 130–138. https://doi.org/10.1016/j.jhazmat.2012.10.010.

Neczaj, E., Grosser, A., 2018. Circular economy in wastewater treatment plant–challenges and barriers. Proceedings 2, 614. https://doi.org/10.3390/proceedings2110614.

Ni, S., Zhou, T., Zhang, H., Cao, Y., Yang, P., 2018. $BiOI/BiVO_4$ Two-dimensional heteronanostructures for visible-light photocatalytic degradation of rhodamine B. ACS Appl. Nano Mater. 1, 5128–5141. https://doi.org/10.1021/acsanm.8b01161.

Orimolade, B.O., Arotiba, O.A., 2020a. Bismuth vanadate in photoelectrocatalytic water treatment systems for the degradation of organics: a review on recent trends. J. Electroanal. Chem. 878, 114724 https://doi.org/10.1016/j.jelechem.2020.114724.

Orimolade, B.O., Arotiba, O.A., 2020c. Towards visible light driven photoelectrocatalysis for water treatment: application of a $FTO/BiVO_4/Ag_2S$ heterojunction anode for the removal of emerging pharmaceutical pollutants. Sci. Rep. 10, 5348. https://doi.org/10.1038/s41598-020-62425-w.

Orimolade, B.O., Koiki, B.A., Peleyeju, G.M., Arotiba, O.A., 2019a. Visible light driven photoelectrocatalysis on a $FTO/BiVO_4/BiOI$ anode for water treatment involving emerging pharmaceutical pollutants. Electrochim. Acta 307, 285–292. https://doi.org/10.1016/j.electacta.2019.03.217.

Orimolade, B.O., Koiki, B.A., Zwane, B.N., Peleyeju, G.M., Mabuba, N., Arotiba, O.A., 2019b. Interrogating solar photoelectrocatalysis on an exfoliated graphite–$BiVO_4$/ZnO composite electrode towards water treatment. RSC Adv. 9, 16586–16595. https://doi.org/10.1039/C9RA02366F.

Orimolade, B.O., Zwane, B.N., Koiki, B.A., Tshwenya, L., Peleyeju, G.M., Mabuba, N., Zhou, M., Arotiba, O.A., 2020. Solar photoelectrocatalytic degradation of ciprofloxacin at a $FTO/BiVO_4/MnO_2$ anode: kinetics, intermediate products and degradation pathway studies. J. Environ. Chem. Eng. 8, 103607 https://doi.org/10.1016/j.jece.2019.103607.

Ouarda, Y., 2020. Electro-oxidation of secondary effluents from various wastewater plants for the removal of acetaminophen and dissolved organic matter. Sci. Total Environ. 8.

Pearson, R.G., 1988. Absolute electronegativity and hardness: application to inorganic chemistry. Inorg. Chem. 27, 734–740. https://doi.org/10.1021/ic00277a030.

Petrie, B., Barden, R., Kasprzyk-Hordern, B., 2015. A review on emerging contaminants in wastewaters and the environment: current knowledge, understudied areas and recommendations for future monitoring. Water Res. 72, 3–27. https://doi.org/10.1016/j.watres.2014.08.053.

Phong Vo, H.N., Le, G.K., Hong Nguyen, T.M., Bui, X.-T., Nguyen, K.H., Rene, E.R., Vo, T. D.H., Thanh Cao, N.-D., Mohan, R., 2019. Acetaminophen micropollutant: historical and current occurrences, toxicity, removal strategies and transformation pathways in different environments. Chemosphere 236, 124391. https://doi.org/10.1016/j.chemosphere.2019.124391.

Puyol, D., Batstone, D.J., Hülsen, T., Astals, S., Peces, M., Krömer, J.O., 2017. Resource recovery from wastewater by biological technologies: opportunities, challenges, and prospects. Front. Microbiol. 7.

Rajeswari, S., Venckatesh, R., 2021. Chapter 24 - ZnO-based nanoparticles for wastewater treatment: a review. In: Abd-Elsalam, K.A. (Ed.), Zinc-based Nanostructures for Environmental and Agricultural Applications, Nanobiotechnology for Plant Protection. Elsevier, pp. 485–507. https://doi.org/10.1016/B978-0-12-822836-4.00022-7.

Ratola, N., Cincinelli, A., Alves, A., Katsoyiannis, A., 2012. Occurrence of organic microcontaminants in the wastewater treatment process. A mini review. J. Hazard. Mater. 239, 1–18. https://doi.org/10.1016/j.jhazmat.2012.05.040. –240.

Rogowska, J., Cieszynska-Semenowicz, M., Ratajczyk, W., Wolska, L., 2020. Micropollutants in treated wastewater. Ambio 49, 487–503. https://doi.org/10.1007/s13280-019-01219-5.

Sajid, M., Bari, S., Saif Ur Rehman, M., Ashfaq, M., Guoliang, Y., Mustafa, G., 2022. Adsorption characteristics of paracetamol removal onto activated carbon prepared from cannabis sativum hemp. Alex. Eng. J. 61, 7203–7212. https://doi.org/10.1016/j.aej.2021.12.060.

Shao, H., Wang, Yanbin, Zeng, H., Zhang, J., Wang, Yan, Sillanpää, M., Zhao, X., 2020a. Enhanced photoelectrocatalytic degradation of bisphenol a by $BiVO_4$ photoanode coupling with peroxymonosulfate. J. Hazard Mater. 394, 121105 https://doi.org/10.1016/j.jhazmat.2019.121105.

Shao, H., Wang, Yanbin, Zeng, H., Zhang, J., Wang, Yan, Sillanpää, M., Zhao, X., 2020b. Enhanced photoelectrocatalytic degradation of bisphenol a by $BiVO_4$ photoanode coupling with peroxymonosulfate. J. Hazard Mater. 394, 121105 https://doi.org/10.1016/j.jhazmat.2019.121105.

Smol, M., Adam, C., Preisner, M., 2020. Circular economy model framework in the European water and wastewater sector. J. Mater. Cycles Waste Manag. 22, 682–697. https://doi.org/10.1007/s10163-019-00960-z.

Sponza, D.T., Oztekin, R., 2016. Treatment of olive mill wastewater by photooxidation with ZrO_2-doped $TiO2_2$ nanocomposite and its reuse capability. Environ. Technol. 37, 865–879. https://doi.org/10.1080/09593330.2015.1088579.

Tang, W., Zhang, Y., Guo, H., Liu, Y., 2019. Heterogeneous activation of peroxymonosulfate for bisphenol AF degradation with $BiOI_{0.5}$ $Cl_{0.5}$. RSC Adv. 9, 14060–14071. https://doi.org/10.1039/C9RA01687B.

THE 17 GOALS. n.d. URL Sustain. Dev., 2023 7.21.22 https://sdgs.un.org/goals accessed.

van der Hoek, J.P., Bertelkamp, C., Verliefde, A.R.D., Singhal, N., 2014. Drinking water treatment technologies in Europe: state of the art – challenges – research needs. J. Water Supply Res. Technol. - Aqua 63, 124–130. https://doi.org/10.2166/aqua.2013.007.

Vogna, D., Marotta, R., Napolitano, A., d'Ischia, M., 2002. Advanced oxidation chemistry of paracetamol. UV/H_2O_2-induced hydroxylation/degradation pathways and 15N-aided inventory of nitrogenous breakdown products. J. Org. Chem. 67, 6143–6151. https://doi.org/10.1021/jo025604v.

Wang, K., Liang, G., Waqas, M., Yang, B., Xiao, K., Zhu, C., Zhang, J., 2020. Peroxymonosulfate enhanced photoelectrocatalytic degradation of ofloxacin using

an easily coated cathode. Sep. Purif. Technol. 236, 116301 https://doi.org/10.1016/j.seppur.2019.116301.
Xiang, Z., Wang, Y., Zhang, D., Ju, P., 2016. BiOI/$BiVO_4$ p-n heterojunction with enhanced photocatalytic activity under visible-light irradiation. J. Ind. Eng. Chem. 40, 83–92. https://doi.org/10.1016/j.jiec.2016.06.009.
Xiao, X., Lin, Y., Pan, B., Fan, W., Huang, Y., 2018. Photocatalytic degradation of methyl orange by BiOI/$Bi4O_5I_2$ microspheres under visible light irradiation. Inorg. Chem. Commun. 93, 65–68. https://doi.org/10.1016/j.inoche.2018.05.009.
Zhang, Y., Shi, L., Geng, Z., Ren, T., Yang, Z., 2019. The improvement of photocatalysis O_2 production over $BiVO_4$ with amorphous FeOOH shell modification. Sci. Rep. 9, 19090 https://doi.org/10.1038/s41598-019-54940-2.